WELDING RESEARCH

SUPPLEMENT TO THE *WELDING JOURNAL*, JUNE 2007
Sponsored by the American Welding Society and the Welding Research Council

Tensile and Fracture Behavior of Pulsed Gas Metal Arc-Welded Al-Cu-Li

At a given mean current, the pulse frequency affects the yield strength of pulsed gas metal arc-welded Al-Cu-Li alloy

BY G. PADMANABHAM, M. SCHAPER, S. PANDEY, AND E. SIMMCHEN

ABSTRACT. Thick plates of Al-Cu-Li-Mg-Ag-Zr-type alloy were butt-joint welded with pulsed gas metal arc welding (GMAW-P). The joints were made at different pulse frequencies but using one drop detachment per pulse (ODPP) condition. Effect of pulse frequency on microstructure, microhardness, tensile strength, and crack growth resistance as well as fracture path were studied. Some laser-welded joints of the same material were also made for comparison purposes. It was observed that the mechanical properties of the joints made with GMAW-P were comparable to the laser welded joints as well as the ones reported in the literature. At the same time, the GMAW-P joints showed reduction in yield strength with increase in pulse frequency. The fracture path also was found to be different with specimens made at different frequencies.

Introduction

Every 1% of Li addition (up to the 4.2% Li solubility limit) to aluminum reduces the alloy density by about 3% and increases the elastic modulus by about 6% L, making aluminum-lithium alloys strong candidates for high-strength low-weight applications like aerospace (Ref. 1). These alloys in welded form could be used to further lighten the structures with weight savings up to 18% (Ref. 2). In the 1980s, the attraction of the light weight of Al-Li alloys prompted development of "second generation" Al-Li alloys 2090 and 8090 to replace conventional aerospace alloys like 2024 and 7075. They contained more than 2% of Li. They had the advantages of lower density, higher modulus of elasticity, and higher fatigue life. But they also had disadvantages like lower short-transverse fracture toughness and higher anisotropy of tensile properties. Weldability was not considered important in developing these alloys. These and other considerations gave rise in the late 1980s and early 1990s to the development of alloys with reduced Li concentration (from 1–1.8%), higher Cu concentration and other alloying elements. These are the third generation of Al-Cu-Li-Mg-Ag-Zr Weldalite™-type alloys 2094, 2095, 2195, 2096, 2097, and 2197. Out of these, 2195 and 2097 have been used in welded applications such as cryotankage and fighter aircraft bulkhead (Ref. 3). In terms of physical metallurgy of these alloys, magnesium and copper contribute to solid solution and precipitation strengthening as well as minimize precipitate free zone formation near grain boundaries. Strengthening precipitates are T_1 (Al_2Cu Li), δ' (Al_3Li), and θ' (Al_2Cu). The β'-Al_3Zr or α'-$Al_3(Zr,Li)$ precipitates act as nucleation sites in addition to grain refinement. Overall, Weldalite-type alloys have an extraordinary natural aging response typically providing longitudinal tensile strength of 590 MPa in T4 temper along with good weldability (Ref. 4).

Weldable high-strength alloys in thick sections could be very useful not only for aerospace applications but also for marine applications, lightweight pressure vessels, and armored land vehicles. Hence, for accomplishing wider application, weldability should be extensively studied. Welding Li-containing aluminum alloys with processes like gas metal arc welding (GMAW), gas tungsten arc welding (GTAW), variable polarity plasma arc welding (VPPA), electron beam welding (EBW), laser beam welding (LBW), resistance welding (RW), and friction stir welding (FSW) have been reported in the literature (Refs. 4–8). Even though the power beam welding processes seem to be yielding better weldment strengths compared to that with arc welding processes, they have certain disadvantages like high accuracy of joint fitup needed, transverse heat-affected zone (HAZ) tearing, large pores and high cost. Another aspect of Al-Li alloys is reduction in thermal conductivity with Li addition, opening the possibility to weld with low-energy-density processes. Therefore, for wider application, it was felt that welding these alloys using the arc welding process in thicker sections might be looked into more closely. The weldable Al-Cu-Li-Mg-Ag-Zr-type alloys were chosen for the investigations, but the formation of a joint weakening equiaxed grain zone (EQZ) at the weld interface (Ref. 9) is an important issue to be addressed in these alloys. Gutierrez et al. (Ref. 10) proposed a

G. PADMANABHAM (gp@arci.res.in) *is scientist-G, International Advanced Research Center for Powder Metallurgy & New Materials, Hyderabad, India. M. SCHAPER* (michael.schaper@mailbox.tu-dresden.de) *is professor, Institute of Materials Science, Dresden University of Technology, Dresden, Germany. S. PANDEY* (pandeysunil@hotmail.com) *is associate professor of Mechanical Engineering, Indian Institute of Technology, New Delhi, India. E. SIMMCHEN* (elke.simmchen@mailbox.tu-dresden.de) *is scientist, Institute of Materials Science, Dresden University of Technology, Dresden, Germany.*

KEYWORDS

Aluminum-Lithium
Al-Li
Gas Metal Arc
Pulsed Arc
Pulse Frequency
Aluminum Alloys

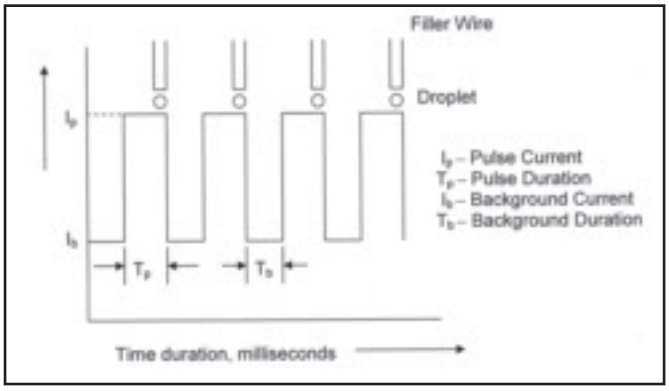

Fig. 1 — Schematic of pulsed current structure in GMAW-P showing one droplet detachment per pulse (ODPP) condition.

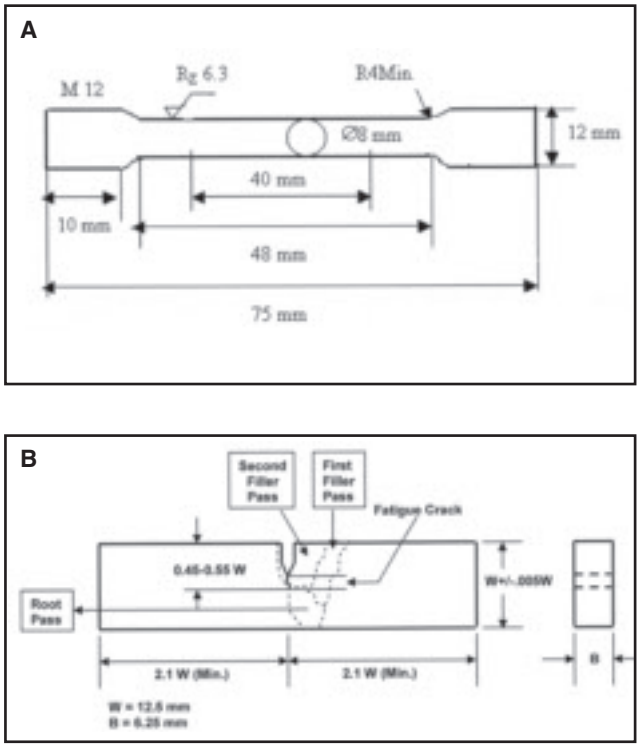

Fig. 2 — Schematic of mechanical test specimens. A — Tensile test specimen; B — K_{Ic} tests Bend Specimen SE(B) indicating the weld and location of precrack.

mechanism for formation of the EQZ and pointed out that the narrow liquid layer that forms into EQZ could be eliminated by enhanced weld pool stirring. In another study using a multigravity research welding system (MGRWS), elevated gravity levels resulted in elimination of the EQZ by promoting rapid mixing throughout the weld pool and dissolution of precipitates, which are believed to be responsible for EQZ formation (Ref. 11).

Gas metal arc welding (GMAW) comes as a preliminary choice when welding thicker sections with high productivity. But it has certain disadvantages like very high heat input, which may result in wide heat-affected zone (HAZ). Pulsed gas metal arc welding (GMAW-P) is known to provide spray transfer conditions at relatively lower mean currents viz., currents below the spray transition current and for a given heat input per unit length of weld the pulsed arc gives a narrower and deeper fusion zone compared with steady GMAW operation, and the HAZ is smaller with less loss of alloy elements due to volatilization (Ref. 12). In GMAW-P, controlled metal transfer is possible at low mean currents (Refs. 13, 14). The pulse parameters can be adjusted to control the droplet transfer mode, heat input, droplet size, or droplet velocities for different welding situations (Ref. 15). This type of flexibility is not possible for conventional GMAW. Welding wire melt-off rate per ampere is more in GMAW-P compared to steady GMAW above the transition current, as proportionately more heat is transferred to the filler metal in GMAW-P than in steady GMAW (Ref. 16). This means better heat transfer efficiency into the weld pool. Additionally, in GMAW-P, high pulse currents result in high electromagnetic forces, which in turn may promote mixing in the bulk of the weld pool (Ref. 17). The filler metal added to the center of the top surface can be quickly transferred to the bottom of the weld pool, then pushed up to the top surface along the fusion boundary and finally driven back to the center (Ref. 18). Enhanced weld metal convection/fluid flow may affect the fusion zone (including EQZ).

Accordingly, experiments were done by

Table 1 — Measured Chemical Composition of Al-Cu-Li Base Metal and 2319 Filler Metal

Element, wt-%	Base Al-Cu-Li Alloy	2319 Filler Metal
Cu	4.45	6.10
Li	1.18	—
Mg	0.48	Traces
Ag	0.44	—
Zr	0.14	0.13
Mn	—	0.28
Si	—	0.05
V	—	0.07
Fe	—	0.12

Table 2 — Common Welding Parameters during GMAW-P Experiments

Mean current	214–218 A
Arc voltage	23–24 V
Peak current	380 A
Peak duration	2 ms
Welding speed	45 cm/min
Shielding gas	Argon 18 L/min (nozzle dia. 17 mm)
Nozzle-to-plate distance	15 mm
Arc length	~6–8 mm
Expected penetration	4.5 mm (Ref. 20) (from bead-on-plate mathematical models) (Ref. 20)
Joint edge preparation	V joint (60-deg groove angle) Root face - 4 mm; root opening - 0.5 mm
No. of passes	1 root pass, 2 fill passes
Backing plate	SS (Groove, 1 mm deep; 5 mm wide)

varying metal droplet transfer frequency with the pulse frequency. Varying pulse frequency here means changing the pulse structure keeping the mean current constant, so that the effect of pulse frequency will be known. Pulse structure at a given mean current has insignificant influence on wire feed rate, hence similar in overall heat input into the weldment (Ref. 19). Even though GMAW-P is generally used for welding thin plates, it has been shown to be useful in welding thicker plates of Al-Cu-Li and that the pulse parameters had some effect on bead geometry and microstructure of the welded joints (Refs. 20, 21). While the general effects of pulsing at various frequencies could be applicable to other alloys also, the effect on EQZ was of interest in the case of the Al-Cu-Li alloy being investigated in this study. In view of the above, GMAW-P seemed to have promise in terms of metallurgical and technological advantages for this type of alloy, including low cost. Therefore, investigations on welding of thick plates of Al-Cu-Li-Mg-Ag-Zr alloys with GMAW-P and some laser welding experiments for comparison were done. Hardness measurements, tensile tests, metallography, fractography, and a few fracture toughness and fatigue tests were carried out.

Experimental Details

In this experiment, the base metal was 13.7 × 50 × 200 mm and made of an experimental alloy (Table 1) in the W and T6 conditions. The welding wire was 1.6-mm-diameter 2319 alloy (Table 1).

The recommended welding parameters and joint design for welding 13.7-mm-thick aluminum plates with GMAW (Ref. 22) is a single-V groove of 60 deg with a backing plate. It prescribes a root face of about 1.5–2.5 mm. But higher root thicknesses have been successfully used for aluminum alloys (Ref. 23) and higher penetration was observed in GMAW-P (Ref. 20). So, a root face dimension of 4 mm was chosen with a view to minimizing filler metal dilution. The base metal plates were dry machined to obtain necessary edge patterns. Surface layers up to 0.2 mm were removed from the locations of welding. The plates were held in position by clamping in the middle of the length direction of the plates with one clamp on each side. Clamping was used during all the weld passes. While this helps in maintaining good ground contact and keeping the two parts in position, it may have resulted in residual stresses. Welding was carried out in the rolling direction of the plates within a few hours of edge preparation.

The parameters for GMAW-P were carried out with direct current (DC) electrode positive polarity (DCEP) using a

Table 3 — Experimental Parameters with Variable Pulse Frequency, with Mean Current Constant

S. No	Pulse Frequency Hz	Peak Current A	Peak Duration ms	Base Current A
X	100	380	2	189
A	125	380	2	173
B	167	380	2	147
C	208	380	2	106
D	250	380	2	60

Table 4 — Laser Welding Experimental Details

Laser power used	3.5 kW
Wavelength	10.6 μm
Raw beam diameter	25 mm
F-factor	8
Mirror focal length	200 mm
Beam radius at focal point	110 μm
Top shielding gas	He, 35 L/min
Back shielding	Argon
Welding plane	Focal plane
Beam quality, K	0.9
Gas nozzle and welding wire feed	45-deg angle with the welding plane
Joint design	Square butt with welding from both sides

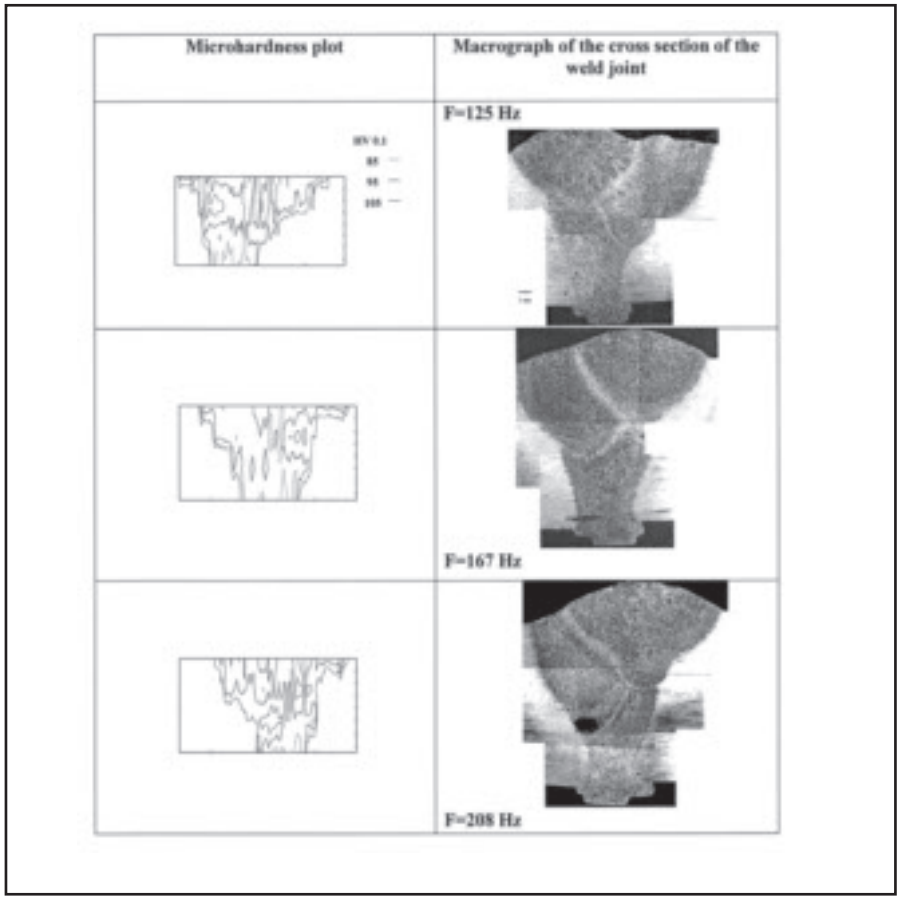

Fig. 3 — Vickers microhardness contour plots and corresponding macrographs of transverse cross sections of the joints made at different pulse frequencies F = 125, 167, and 208 Hz.

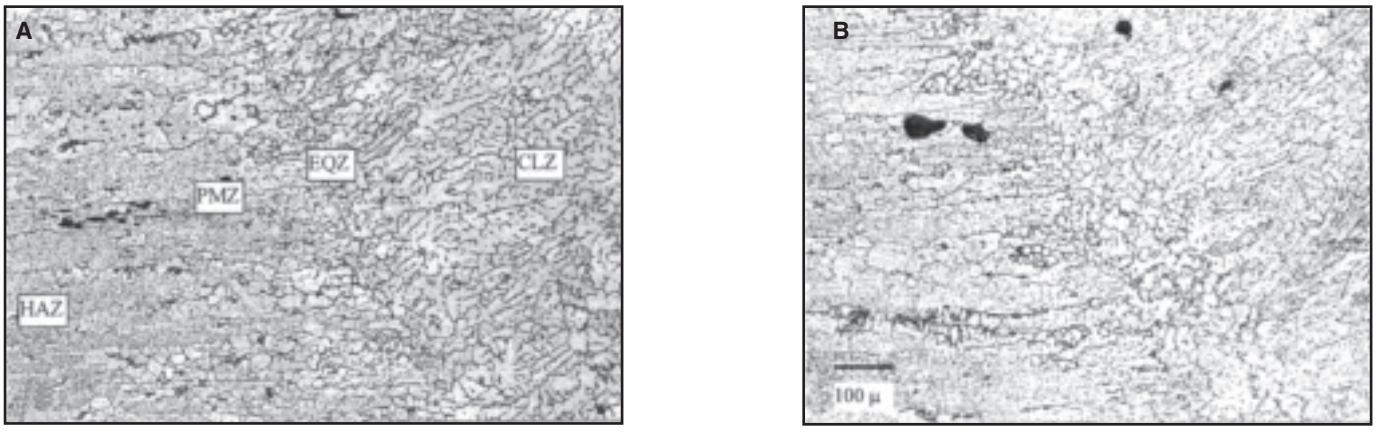

Fig. 4 — Microstructure near fusion boundary of root pass weld (cross section) in as-welded condition for various pulse frequencies. A — 125 Hz; B — 167 Hz; C — 208 Hz. EQZ = Fine equiaxed grain zone; PMZ = partially melted zone; CLZ = columnar zone; and HAZ = heat-affected zone.

transistorized power source. The output V/A slope of the welding power source was set in constant current condition. Mechanized GMAW station was employed for depositing weld beads. An arc length of about 6–8 mm was maintained during all the experiments through manual control of wire feed speed. Based on some preliminary experimental trials and parameters as per handbooks, welding parameters as given in Table 2 were chosen. Joints were made in three passes: one root pass and two filler passes. Between the passes, enough time was allowed to bring the specimens to ambient temperature. Throughout the experimentation, the overall heat input per unit length was kept constant by keeping the mean current, arc voltage, and welding speed the same. One drop per pulse (ODPP) mode of detachment with droplet detachment at the end of the pulse was used — Fig. 1. Pulse parameters were fixed and background conditions varied based on the calculated parameters determined using the following equations (Ref. 20):

$$W_f \text{ (m/min) (wire feed rate)} = 0.0258\ (I_m) \quad (1)$$

Equation 1 is an experimentally determined relation between welding wire feed rate and mean current to meet the melt-off criterion to obtain a stable arc (viz., sufficient amount of welding wire is fed equaling the melting during welding so that a stable welding arc is maintained). Using this equation, the required wire feed rate (W_f) is determined for a particular mean current (I_m), of which I_m = 215 A and W_f = 5.6 m/min were used in all the experiments. In spray transfer mode, metal transfer with the diameter of the transferring droplet equal to or less than the diameter of the welding wire is preferred. Assuming negligible material losses due to spatter, the volume of wire melted ($W_f \times \pi\ r^2$ wherein r is the radius of the welding wire) divided by the volume of single droplet ($4/3\ \pi\ r_d^3$ where r_d is the radius of the droplet) will yield the frequency (F), which is the same as pulse frequency F in case of ODPP condition of metal transfer. This can be represented as Equation 2 below.

$$W_f \times \pi\ r^2 = F \times 4/3\ \pi\ r_d^3 \quad (2)$$

Relation between pulse frequency F, total cycle time T, pulse duration T_p, and base current duration T_b is given by Equations 3 and 4.

$$F \text{ (pulse frequency)} = 1/T \quad (3)$$

$$T \text{ (Total pulse cycle time)} = T_p + T_b \quad (4)$$

Using Equations 1–4, for a particular mean current and possible pulse frequencies (consequently total pulse cycle time) for droplet radius equal to or less than the wire radius can be determined. The relation between I_p and T_p (pulse current and duration) is known to follow a power law for achieving the ODPP condition as shown in Fig. 1. This relation experimentally determined for the 2319 alloy welding wire (Ref. 20) is as follows:

$$I_p^{1.4}\ T_p = 8857\ A^{1.4}.ms \quad (5)$$

For a given pulse current, pulse duration can be determined by Equation 5. At a given mean current and pulse frequency, using Equations 1–5, values of I_p, T_p, and T_b values can be calculated. The mean current and pulse parameters are related as per Equation 6 below.

$$I_m \text{ (Mean Current)} = (I_p T_p + I_b T_b)/T \quad (6)$$

Using Equation 6 the value of T_b can be determined.

Based on the above relations and calculation using these equations, the GMAW-P parameters for various possible sets of experiments (X, A, B, C, and D) for different pulse frequencies for a condition where the detached droplet diameter is equal to or less than the diameter of the welding wire are given in Table 3. For the same mean current, pulse frequency is increased from a particular value. This implies detachment of more droplets keeping the mean current/wire feed rate constant. The aim was to vary the metal transfer conditions keeping the mean current constant. As the welding speed also was kept constant in all the cases, the overall heat input into the weld is expected to be the same. While using parameters X in Table 3, the voltage transient showed some droplet detachments during the background conditions as well. The welding conditions also were not good in terms of arc stability and noise. It was thought that background current being in the spray

transition current range of 177–190 A for the 1.6-mm-diameter 2319 filler metal (Ref. 20) might be the cause of multiple droplet detachments. Hence, this set of parameters was not used for final experiments. Also, with parameter set D, the arc was unstable and the root fusion was inadequate. There seems to be a practical frequency limit beyond which there are no feasible pulse parameters for smooth welding at a particular mean current. While this limit was around 170 Hz for mean current of 195 A (Ref. 21), it seems to be around 250 Hz for 215 A. This needs to be further investigated. Hence, sets of parameters A, B, and C with background current substantially below 190 A, which is the spray transition current for the 1.6 mm 2319 filler metal, were chosen for final experiments.

Laser Welding

A Rofin sinar DC035, 3.5-kW slab laser machine was used for the welding experiments. Welding was carried out in keyhole mode at a speed of 30 cm/min at 3.5 kW of power, which gave a maximum penetration of 7 mm. As the plate thickness was about 13 mm after surface preparation, welding was conducted from both sides with square-edge butt joint preparation. The mating surfaces were dry machined. Helium gas shielding at a flow rate of 35 L/min was used. Welding wire was fed at the rate of 30 cm/min. Full experimental details for laser beam welding are given in Table 4. These were only one set of possible welding parameters, not essentially the optimal welding conditions.

With the above welding conditions, heat input for GMAW-P and laser welding was comparable at 7000 W/cm and 6880 W/cm, respectively.

Base Metal Conditions

In T6 condition, two plates for each parameter set and in W condition, two plates for each parameter set were welded. Due to paucity of material and as T6 is more technologically feasible condition for applications, the laser welding experiments were conducted on plates in T6 condition only.

Welding of W Specimens

Specimens A1, A2, B1 were welded in first batch when the hardness was 68 HRB. Welding of B2, C1, C2 specimens was done in second batch by which time the hardness was 73.5 HRB, due to natural aging. Experiment set A is where pulse frequency F = 125 Hz, B when F = 167 Hz, and C when F = 208 Hz throughout the experimentation. First and second plates A1 and A2 were welded with the same welding conditions, as were B and C. The specimens welded in T6 conditions were numbered with T6 in the beginning, and specimens welded in W condition were numbered W in the beginning. This designation is explained here for ease of discussion in following paragraphs.

Metallography, Hardness Surveys, and Tensile Tests

Standard metallographic practices for grinding and polishing of cross sections of the weld were used. Keller's reagent was used for etching of all the specimens. The line intercept method for grain size measurement was not feasible due to columnar nature of the grains. Hence, only qualitative observations are reported. Vickers microhardness measurements using an automatic hardness tester, which can be programmed in terms of the number of indentations and in the form of a fine grid across the whole specimen cross section was employed. A load of 100 g for 12 s was used to make the indentations. As the main aim of the study was to know the microstructure dependence of the weld properties, transverse tensile specimens of round cross section were machined from the welded plates. This avoided the effects of reinforcement, distortion, etc. Round cross section tensile specimens were made as per DIN 50125 B8X40 (length 40 mm, diameter in the gauge length area 8 mm). Schematic of the tensile specimens is given in Fig. 2A. The crosshead speed used was 1 mm/min. The specimens were lightly etched with Keller's reagent before the tensile test, to be able to see the fracture path vis-à-vis the weldment. Fractography on the broken tensile test specimens was carried out with scanning electron microscope Zeiss DSM 986.

Fatigue and Fracture Toughness Tests

Edge-notched three-point bend specimens were made as per ASTM E 399 (cross-section thickness B = 6.25 mm and width W = 12.5 mm) for fracture toughness (K_{Ic}) determination. The precrack was made by spark cutting a sharp notch and subsequent fatigue cracking such that the final crack tip was positioned at the desired location in the last filler pass. Schematic of the specimen including weld and position of precrack is shown in Fig. 2B. During fatigue precracking, fatigue crack length data were collected and used for both ΔK control according to the prescribed load shedding procedure as well as automatic switch-off of the cyclic load as soon as the crack achieved half width. During the fatigue precracking, fatigue crack growth rates were calculated for selected specimens. Fatigue precracking and crack growth measurements were carried out on a computer-controlled dynamic compliance (DYNACOMP) equipment. The physical principles of this testing machine, experimental procedures, and application examples in fracture research are presented in literature (Ref. 24). With this machine, the specimen is electrodynamically excited to resonance vibrations of controlled amplitude. Because the specimen is excited at its resonance frequency, the specimen compliance and therefore the actual crack length can be almost continuously determined by high-resolution period measurements. Thus, the resonance vibrations serve to both load the specimen and monitor crack length. A load ratio R = 0.5 was used for precracking in order to minimize crack path irregularities, which might result from internal stresses and microstructural effect in the welded zone.

Results and Discussion

Welding conditions in terms of arc stability, spatter, and noise were found to be better with higher frequency welding parameters. But, with parameter set C, the arc stabilization took longer time than for A and B. All the plates have shown distortion. Two plates welded in T6 condition showed cracks in the plane parallel to plate surface, approximately at the center of the thickness. It looked like delamination between grains of the rolled structure through grain boundary melting phases, subjected to residual stresses in the welded plates.

Hardness Survey and Analysis of the Joints

A grid of 17 mm (across the fusion zone at 0.25-mm intervals) × 7.5 mm (in plate thickness direction at an interval of 2.5 mm) was programmed into the automatic Vickers microhardness tester. A total of 288 indentations per weld were made. The hardness values obtained from automatic measurements were used to draw a contour plot of the microhardness across the weld cross section. These contour plots and macrograph of the middle portion of the weld joints where the measurements were done are given in Fig. 3. Hardness at the weld interface in all cases was approximately 100 VHN. The hardness of the second fill pass is higher than the first fill pass, and the first fill pass is harder than the root pass. This is the trend generally observed in all the specimens. As the successive weld beads are being deposited, the earlier weld bead received more heat, which may result in grain coarsening and softening. The areas near the weld bead

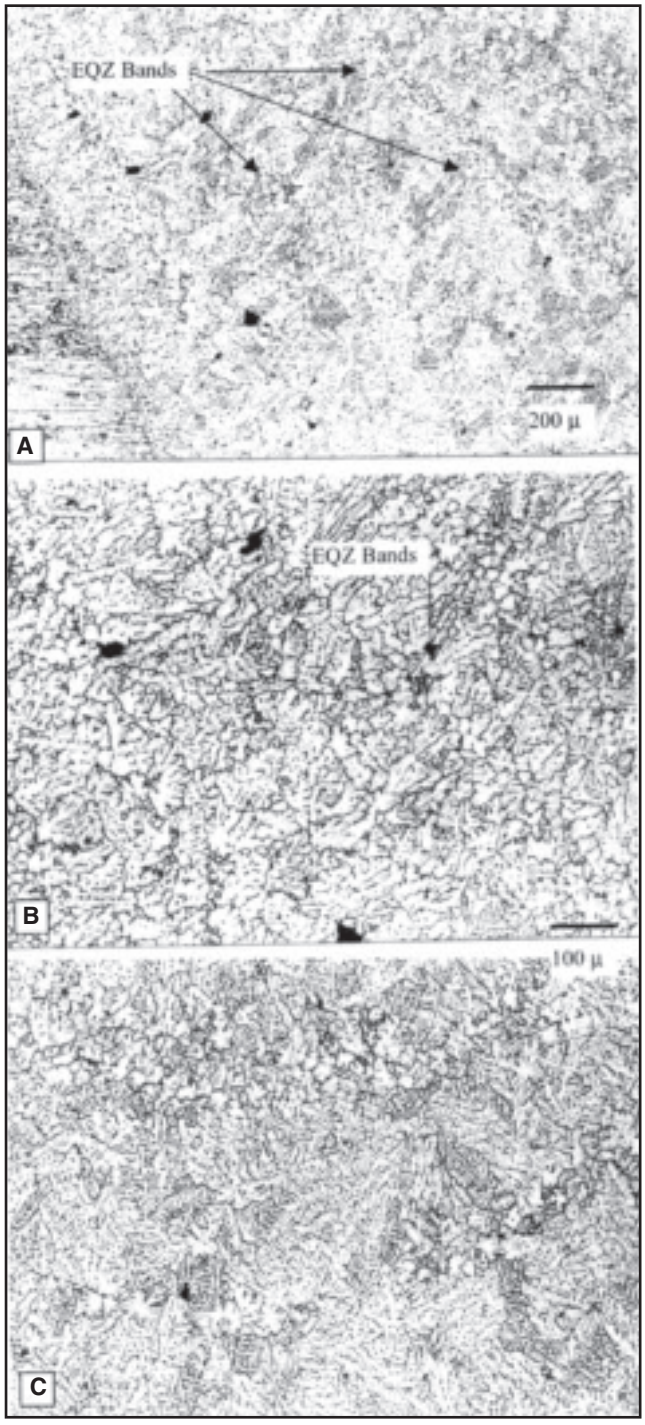

Fig. 5 — EQZ bands seen in the body of the weld in specimen made at pulse frequency 208 Hz. A — Low magnification showing more EQZ bands; B and C — higher magnification of some EQZ bands.

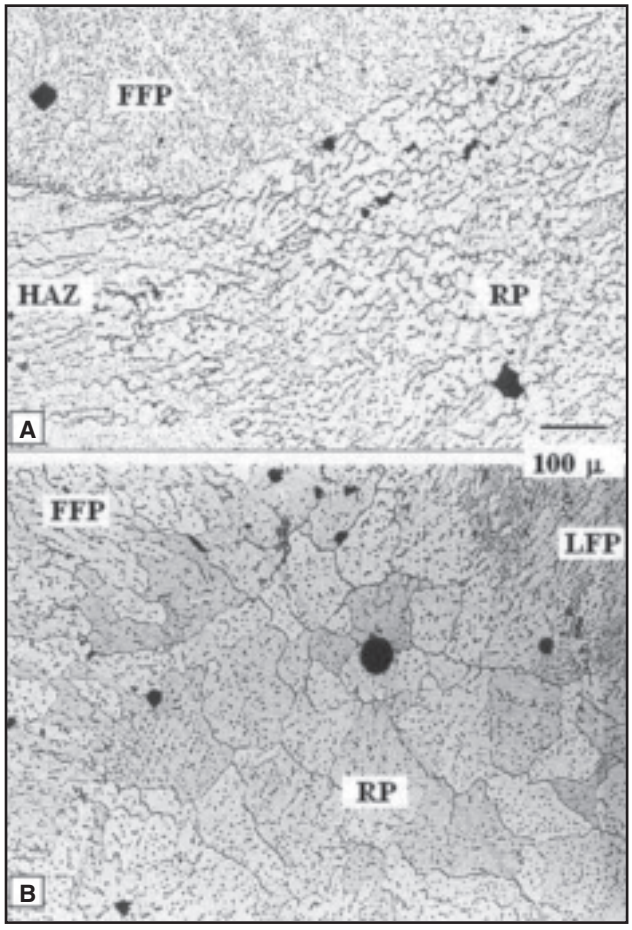

Fig. 6 — Microstructure of cross section of weld made at F = 125 Hz. A — Boundaries of heat-affected zone of base metal (HAZ) – root pass (RP) – first fill pass (FFP); B — boundaries of root pass – first fill pass – last fill pass (LFP).

interface experience this effect more severely. The lowest hardness was observed in the middle of the root pass in all the specimens. With the specimen welded at 125 Hz, low hardness was also observed in first fill pass adjacent to the interface with second fill pass as well as in the middle of the weld bead. With the specimen welded at a frequency of 167 Hz, the lowest hardness was observed at the interface of two fill passes, in the first fill pass, as well as interface of root pass and first fill pass and in the root pass. The same trend was observed in the specimen made at 208 Hz. So, the interfaces between passes could be the low strength areas in the joints.

Porosity was observed in all the weldments. The second fill pass was deposited after cleaning the top of the root and the first fill pass with a stainless steel wire brush. This amount of cleaning was perhaps not enough for these alloys. A large irregular pore was observed with the specimen welded at 208 Hz. As mentioned above, while welding the specimen at this pulse frequency, there was some instability in the arc, which could have resulted in air aspiration resulting in such a pore. The laser welded specimens had pores of irregular shape up to 2 mm in size.

Microstructure

The microstructures of the weld bead cross section near the weld interface of the root pass made at different pulse frequencies are shown in Fig. 4. Grain growth and recrystallization is seen in the heat-affected zone (HAZ). The zone immediately adjacent to the fusion zone is identified as partially melted zone (PMZ), and it had some pores. Specimen A shows more severely affected PMZ. The first region within the fusion zone on the weld interface contains fine equiaxed grains. This is the EQZ. Beyond this EQZ, into the fusion zone the microstructure is dendritic, typical of weld microstructures. The EQZ is only 2–3 grains thick, and in specimen C, bands of EQZ were seen in the fusion zone — Fig. 5. The location where these bands were observed showed absence of the EQZ at the weld interface. This is similar to that observed in the bead-on-plate

Table 5 — Tensile Test Results and Other Observations on Failure Path and Visual Examination of Presence of Pores

Specimen No.	YS, MPa	UTS, MPa	% Elong.	Position of Failure/Fracture Path and Other Observations
			Frequency = 125 Hz	
T6A1-S1	210	255	0.65	Fracture surface showed two large pores of up to 1 mm dia.
T6A1-S2	227	323	2.17	Weld interface – crown side Weld metal – root side
T6A1-S3	213	306	1.9	Weld interface – crown side Weld metal and weld interface – root side,
T6A2-S1	215	314	2.14	Weld metal – crown side (but could be on weld interface of two face passes) Weld interface – root side
T6A2-S2	230	309	1.4	Fusion zone – crown side and root side, But at one place where there was a pore, it was on weld interface.
T6A2-S3	229	278	0.72	Fusion zone – crown side and root side, but at one place where there was a pore, it was on weld interface.
WA1S1	237	316	2.21	Through last fill pass to weld interface and along weld interface on root pass
WA1S2	244	309	1.32	Through second bead and weld interface of root pass
WA2S1	241	302	1.25	Through last bead to its weld interface and through weld interface of root pass
WA2S2	230	273	0.62	Through first fill pass weld interface with last fill pass and through root pass
			Frequency = 167 Hz	
T6B1-S1	205	315	3	Weld metal – crown side Weld interface – root side
T6B1-S2	230	311	1.57	Through weld metal on the root side. It went through fusion zone for some distance but one end of the fracture seems to on the weld interface.
T6B1-S3	216	279	0.93	Same as above
T6B2-S1	213	305	2	Observable minor porosity on the specimen surface. Fracture path predominantly on weld interface.
T6B2-S2	205	261	1	Through weld metal on crown side ending on weld interface on the root side.
T6B2-S3	216	275	0.86	Fusion zone on crown side extending into weld interface on root side. On root side, fracture seemed to have gone into base metal as well.
T6B2-S4	208	276	1.1	Crown side – fusion zone (could be on weld interface of two face passes) Root side – weld interface
WB1-S1	212	334	4.13	Through first face pass up to weld interface with base metal and through weld interface of root pass
WB1-S2	204	323	2.18	Same as above
WB2-S1	205	289	2.1	Mostly through fusion zone, across the large pores
WB2S2	218	324	2.94	Through first face pass to weld interface with base metal and along the weld interface up to end of root pass
			Frequency = 208 Hz	
T6C1-S2	—	—	—	Fusion defect in the specimen. Not suitable for testing.
T6C1-S3	203	296	1.9	Two large pores on fracture surface. Fracture path predominantly in fusion zone.
T6C1-S4	—	—	—	Fusion defect in the specimen
T6C2-S1				Fusion defect in the specimen. Not suitable for testing.
T6C2-S2	210	326	3.36	One large pore of dia. 1 mm in the fracture surface. Fracture through fusion zone on crown side and weld interface root side.
T6C2-S3	205	323	3.68	Fracture path similar to T6C2-S2 above
T6C2-S4	200	289		One pore of 0.5 mm dia. Crown side – fusion zone Root side – weld interface
WC1-S1	207	291	1.94	Fracture through first face pass and through root pass. Path seems to be decided by presence of pores
WC1-S2	210	281	1.89	Same as above
WC2-S1	208	265	1.69	Same as above
WC2-S2	214	296	1.89	Same as above and ending on weld interface of root pass
			Laser Welded Specimens	
T6A-S1	253	317	1.6	Generally through fusion zone and large pores, touched the weld interface rarely
T6A-S2	241	310	1.59	Same as above
T6B-S1	249	299	1.29	Same as above
T6B-S2	246	316	1.74	Same as above

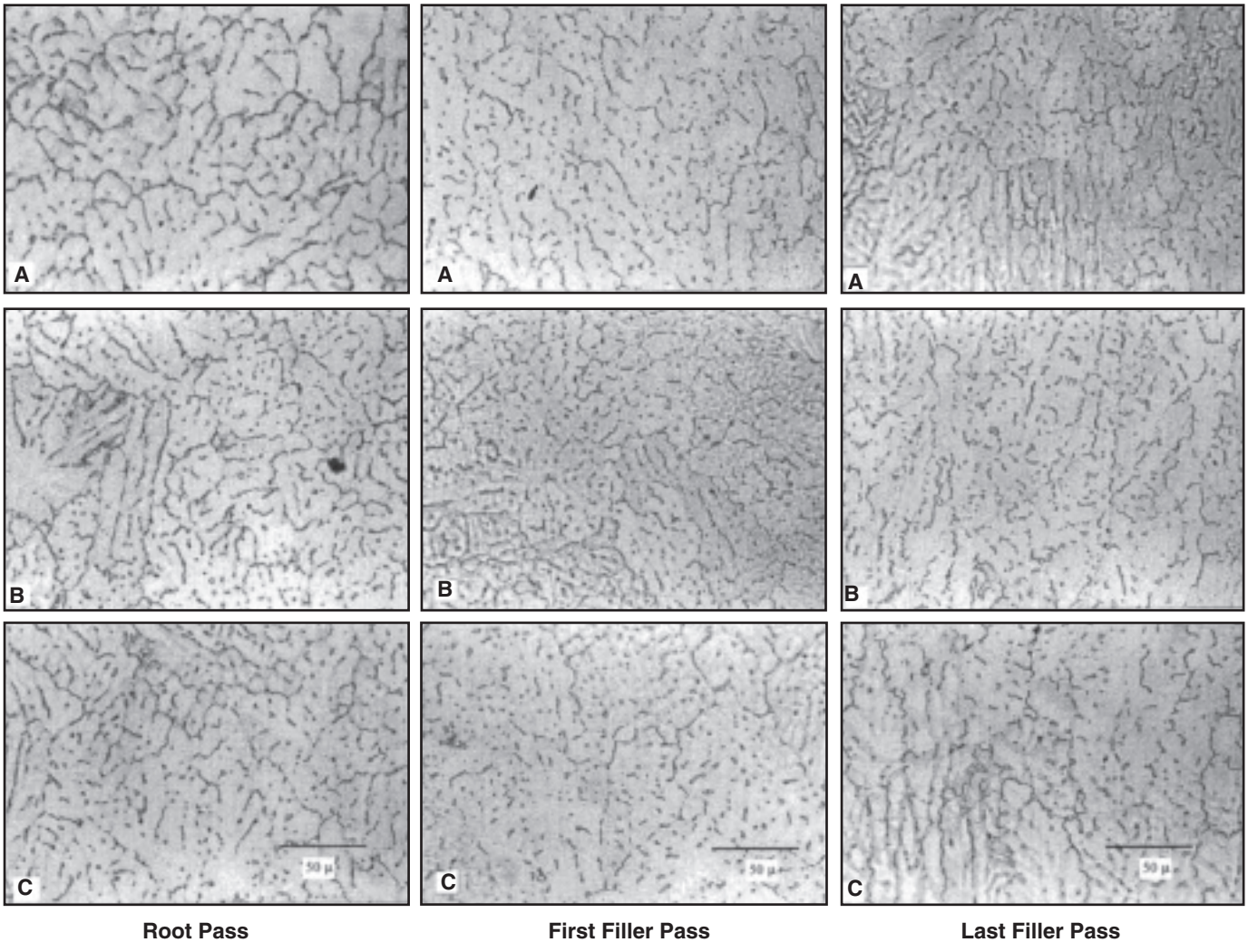

Fig. 7 — Microstructure in the middle of different weld passes in the welds made at different frequencies. A — F = 125 Hz; B — 167 Hz; C — 208 Hz.

Table 6 — Average Transverse Tensile Properties of As-Welded Joints Made of GMAW-P at Different Pulse Frequencies and Laser Welding

Base Metal Condition	Pulse Freq. Hz	Yield Stress, MPa	Fracture Stress, MPa	% Elongation on 40-mm Gauge Length
		Pulsed GMAW		
T6	125	221	298	1.5
	167	213	289	1.5
	208	204	309	2.72
W	125	238	300	1.35
	167	210	318	2.84
	208	210	283	1.85
		Laser Welded		
T6		247	310	1.55

experiments as well (Ref. 21). So, the weld pool convection or fluid flow increase could not only be dragging the EQZ-forming crystallites into the weld, but resulted in low temperatures where the crystallites can survive.

The microstructural features at the boundaries of the weld interface and different weld bead passes are shown in Fig. 6. At the junction of base metal HAZ, root pass and the first fill pass, EQZ can be clearly seen along the weld interface of the root pass, but the same is not the case with the boundary with the first fill pass. First fill pass also shows the EQZ on the weld interface with the base metal but no EQZ at interface with root pass. This was also observed in case of boundaries between any two different weld passes. So, the EQZ is restricted to the weld interface between the weldment and the base metal only. The difference between the weld metal and base metal is that they have undergone different thermomechanical

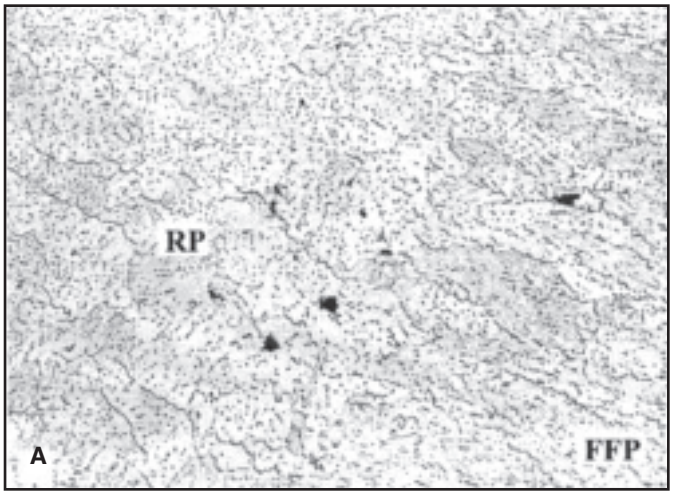

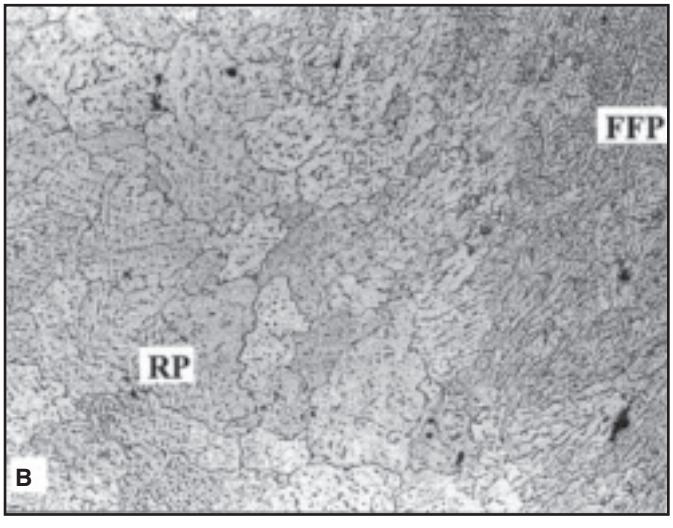

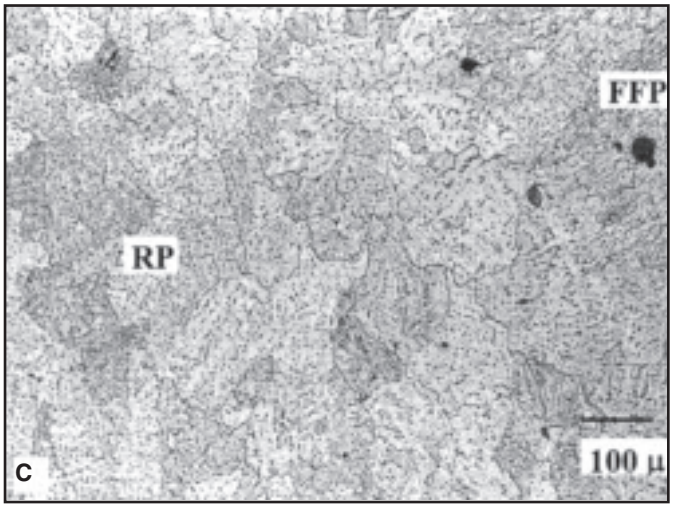

Fig. 8 — Microstructure at the boundary of root pass (RP) and first fill pass (FFP) of welds made at different frequencies. A — 125 Hz; B — 167 Hz; C — 208 Hz.

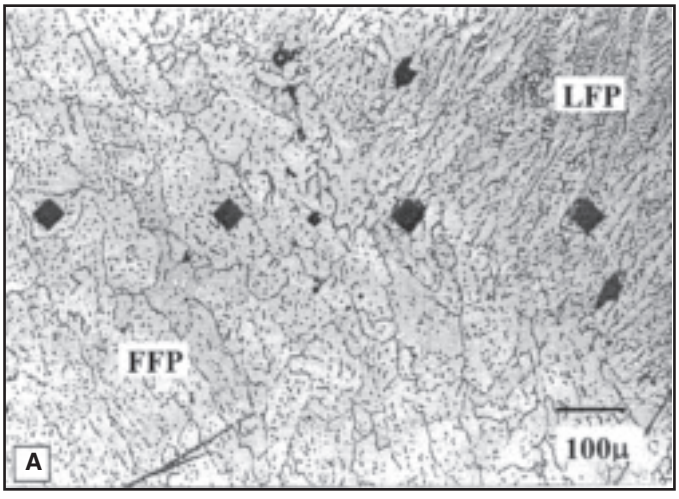

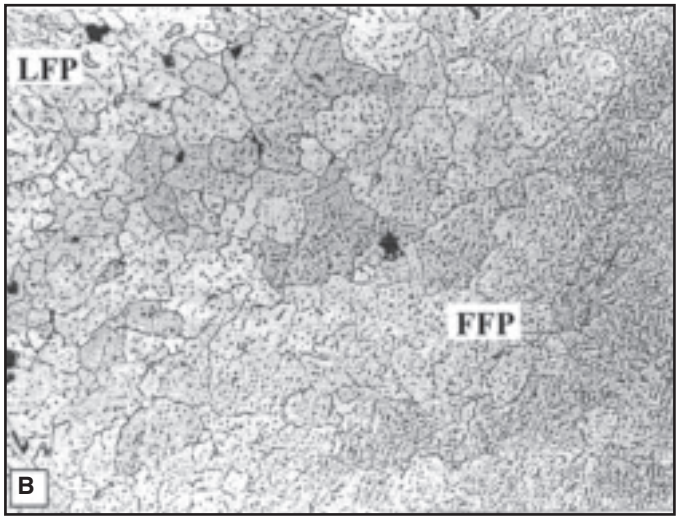

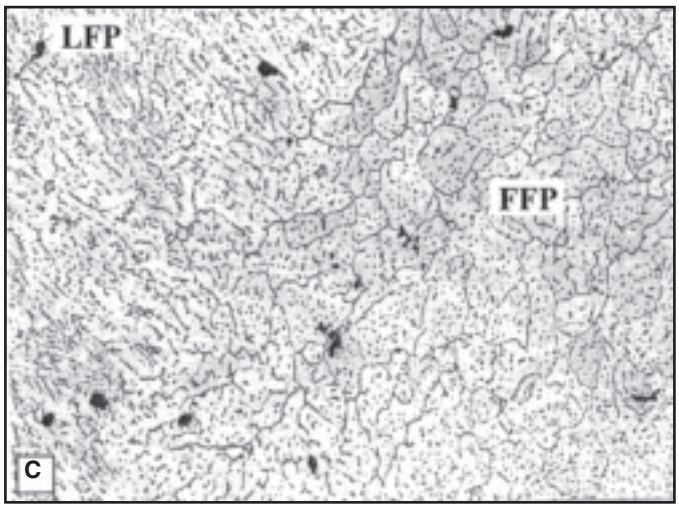

Fig. 9 — Microstructure at the boundary of first fill pass (FFP) and last fill pass (LFP) of welds made at different frequencies. A — 125 Hz; B —167 Hz; C — 208 Hz.

processes. The base metal has a rolled and heat-treated structure and the weld metal a cast structure solidified from high welding temperatures. The EQZ grains are known to form through a heterogeneous nucleation mechanism aided by Al_3Zr and $Al_3(Zr_xLi_{1-x})$ phases. These phases do not survive temperatures above 643°C. Hence, the fusion zone, which has solidified from high temperatures, is not expected to have them. So, the difference between base metal and a solidified weld bead is the presence and absence of these heterogeneous nucleation sites. Hence, at the fusion boundary with the base metal,

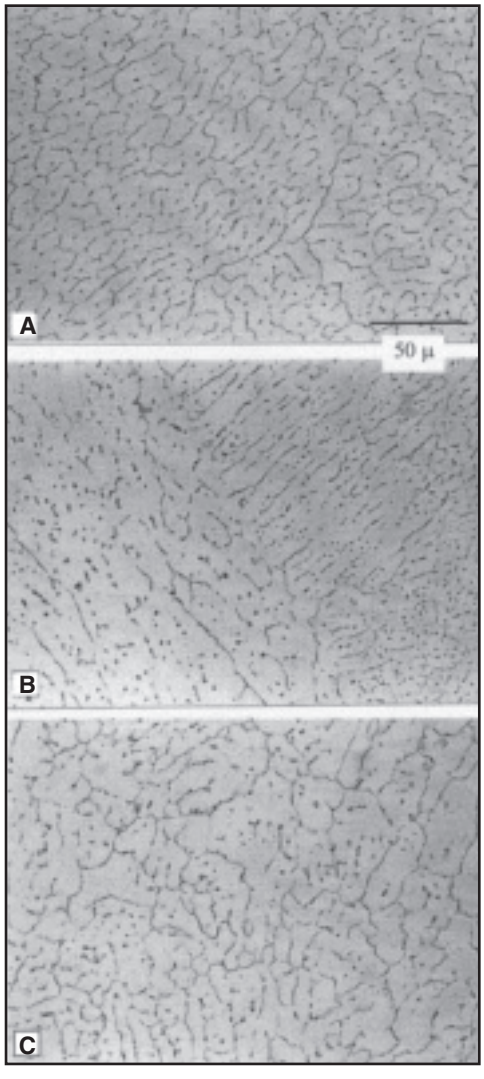

Fig. 10 — Microstructures of cross section of the laser-welded specimen. A — Middle of the first pass; B — boundary of two passes; C — middle of second pass.

the EQZ could form and at the fusion boundary between two weld passes it could not form. This result is similar to that reported by other workers as well (Refs. 10, 30).

Microstructures in the middle of the different passes for specimens made at different frequencies are given in Fig. 7A, B, C. In the first fill pass and the last pass, it is observed that the higher frequency specimen shows coarser dendritic structure (subgrain microstructure) than the lower frequency specimen.

Microstructures of boundary between root pass and first fill pass are shown in Fig. 8. Coarsening of the subgrain structure is very clearly evident in the areas adjacent to the weld interface. Similarly, adjacent to the boundary between the first fill pass and last fill pass, the subgrain structure of the first fill passes have coarsened as shown in Fig. 9. This coarsening effect is higher in the root pass than in the first fill pass due to twice the amount of heat it is exposed to. This result matches with the observation in hardness surveys (Fig. 3) that the hardness value at the junction of first and last fill passes and in the root pass are lower compared to the other areas of the weld. Hence, in the transverse tensile test, this could limit the strength of the joint.

Microstructures of the laser-welded specimen are shown in Fig. 10. The microstructure in the first pass is finer than the final pass and is finer than observed in the GMAW-P specimens. Coarsening of the subgrain structure at the boundary of the two passes was also seen. The laser-welded joints due to high energy density and smaller weld pool are expected to cool faster than the GMAW-P welds. This could be the reason for the finer microstructure.

Tensile Test

Weld specimens welded in T6 and W conditions were tested for tensile properties by machining out transverse specimens. In the specimen designation, the three frequencies were designated as 125 Hz (A), 167 Hz (B), and 208 Hz (C). S1 is the tensile specimen drawn from the beginning of the weldment, S2 from the end of the weldment, S3 and S4 anywhere in the middle. All of them were tested in as-welded condition without any postweld aging treatment. But the testing was done three weeks after welding by which time it was expected that natural aging also could have taken place.

Results of all the tensile tests, i.e., yield strength, fracture stress, and fracture strain as well as observations on the fracture path are given in Table 5. Summary of the tensile test results is given in Table 6. The term fracture stress is used instead of ultimate tensile strength (UTS) for the reason that all the specimens failed during the upward movement of the stress-strain curve. It is the stress at the point of fracture, which is also the point of maximum stress experienced during the tensile test. If significant porosity is present, fracture stress should be affected by the amount of porosity even more than UTS, whereas deformation of the matrix material is best reflected by the yield strength.

The fracture path observations indicate that cracking occurs in most cases through the first fill pass up to the weld interface and along the weld interface of first fill and root passes. This observation is different from what is reported in literature (Ref. 9) that the failure in joints is occurring all along the weld interface in EQZ. It is probably due to weaker material in the first fill pass as seen in the hardness surveys, which is yielding easily when transverse load is applied. The shape of the weld bead is wider on the crown side and narrower on the root side. The weld interface of the root pass is somewhat perpendicular to the tensile testing load and in the fill passes at an angle to the load direction. At the same time, there is a weaker zone in the first face pass as indicated by the hardness surveys. Fracture path includes fusion zone and weld interface as well. In more tensile specimens it is on the weld interface of the root pass and fusion zone of the face passes. In the case of two of the tensile specimens where the fracture on the crown side was on the weld interface the fracture either continued on the weld interface or fusion zone of the root pass (tensile specimens T6A1S2 and A1S3). This shows that weld interface still is a weaker location in these joints, but overall fracture path is dependent on the shape of the weld bead and weaker zones in the weld beads.

In the tensile specimens, which showed significant porosity, the fracture preferred to go through the pores. Such specimens specifically showed lower fracture stress. It is well known that up to a certain level of porosity, the yield strength is unaffected but the fracture stress is affected. Similar effect was seen in the laser welded specimens that had large pores, reducing the effective cross section taking the load. Hence, comparison of yield strength is felt to be more appropriate to compare the effect of microstructure on tensile properties. The yield strength decreased with increase in pulse frequency. This could be due to microstructure becoming coarser with an increase in frequency, observed both in the beads-on-plate experiments as well as on the butt joints. Laser welded specimens, which experience much faster cooling rates, resulted in finer microstructures and yielded better yield stress, but the fracture stress is similar to that of GMAW-P specimens. This again could be due to the large pores in the laser-welded specimens.

The percentage elongation seemed to be increasing with the pulse frequency, but it is only a reflection of the difference between yield point and fracture stress in case of each specimen. The fracture in all the tensile specimens took place in the fusion zone or the weld interface except in the ones containing large pores. As almost all the plastic deformation during tensile test occurred in the fusion zone, the elongation values at fracture are typically of the fusion zone, which is about 17 mm wide, calculated over a 40-mm gauge length. Therefore, the true fracture strain values are higher actually. So, the conventional fracture strain may not be suitable

for comparison.

Tensile properties of butt joints of this experimental alloy made with GMAW-P and similar alloys with other processes are given in Table 7. The tensile properties are comparable with even higher energy density processes like variable polarity plasma arc welding or laser beam welding.

Fractography

Fractography of one of the tensile specimens from a weld made at 125 Hz is shown in Fig. 11. In two areas, the fracture path was through the weld interface. These are shown in Fig. 11A and C. The fractograph Fig. 11A looks like intergranular failure and could be through the EQZ. The fractograph Fig. 11C shows a lamellar structure. This seems to be resembling the partially melted zone (PMZ) seen in the transverse direction to rolling. Other specimens welded with similar frequency also showed some lamellar region. Hence, weld interface fracture path touches the PMZ as well indicating that this is also a weaker zone in these weldments. Figure 11B shows the area in which the fracture was through the middle of the root pass. It shows a ductile fracture. Similarly, the Figs. 12 and 13 show the fractographs of tensile fractures of specimens from welds made at 167 and 208 Hz, respectively. The Fig. 12A, which is in the fusion zone, shows a ductile failure. Figure 12B and C, which are from the weld interface, show a different structure: intergranular structure in Fig. 12B where the fracture could have gone through the EQZ and the lamellar structure in Fig. 12C where the fracture could have gone through PMZ. Figure 13 shows the similar pictures for 208 Hz. Figure 14 compares the fractographs of the specimens made at three different frequencies and where failure is through the fusion zone in similar locations. As the fracture surfaces were uneven, it is difficult to say if it was the exact size of the dimples.

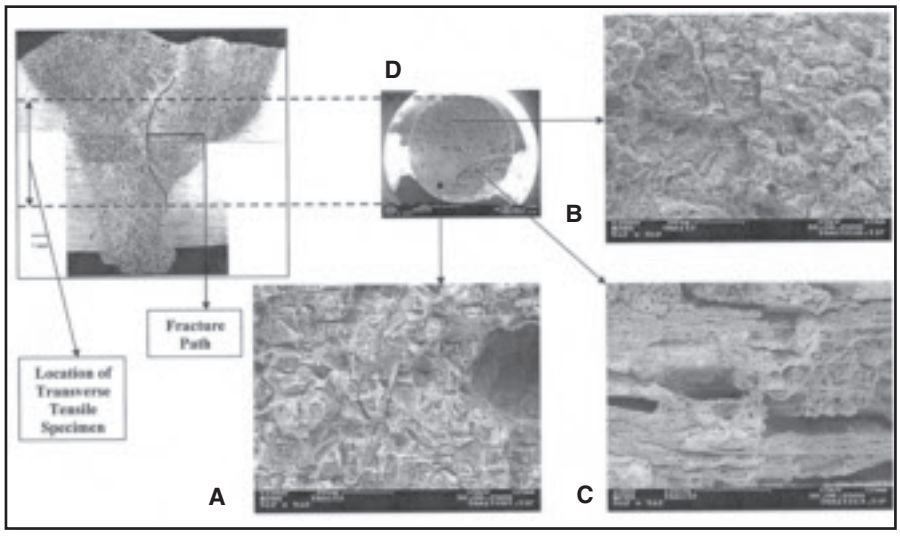

Fig. 11 — Fractograph of broken tensile specimen from weld made at F=125 Hz. A — Fracture path was in the weld interface/boundary of the fusion zone; B — fracture path through fusion zone of root pass; C — weld interface; D — fractured specimen.

Table 7 — Comparison of Tensile Properties of Pulsed-GMA Welded Joints with Values Reported in Literature for Other Welding Processes (Refs. 9, 26, 27)

Process	Material/ Thickness	Filler	Test Condition	0.2% Proof Stress, MPa	UTS, MPa	% Elong. (I_0–50 mm)
Laser welding	2195/3 mm	AlSi12	As welded in T8 condition	285	325	1.1
GTAW	2094-T8	2319	As-welded	—	352	—
VPPAW	2094-T8	2319	As-welded	269	372	—
GMAW	2094-T8	2319	As-welded	—	283	—
EBW	2094-T8	—	As-welded	—	434	—
Pulsed-GMAW Present results	Experimental Alloy-T6/13.7 mm	2319	As-welded	221	298	1.5
Laser welding (Present results)	-do-	2319	As-welded	247	310	1.55

Table 8 — Results of the Linear Regression Analysis of Crack Growth Curves

Specimen No.	Log C (base 10)	m
A1LiT622	–10.48	3.04
A1LiT632	–11.14	4.69
T6A1F1	–10.75	3.37
T6A1F2	–10.93	3.66
T6A2F1	Curve not clear	
T6A2F2	–10.53	2.91
T6B1F1	–10.4	3.04
T6B1F2	–12.62	6.56
T6B2F1	–10.69	3.18
T6B2F2	–10.71	3.22
T6C2F1	–10.6	3.41

Table 9 — K_{IC} Test Results, Undersized Specimens

Specimen No.	K_Q, MPa $\sqrt{m}$
Base metal in T6 condition	
A1LiT621	25.2
A1LiT631	21.3
A1LiT622	24.1
A1LiT612	25.1
A1LiT632	24.6
A1LiT611	25.1
P-GMA welds in three different pulse frequency conditions A, B, and C	
T6A1F1	12.4
T6A1F2	15.7
T6A2F1	13.6
T6A2F2	10.8
T6B1F1	12.7
T7B1F2	13.0
T6B1F3	12.2
T6B2F1	15.4
T6B2F2	13.2
T6C2F1	12.6

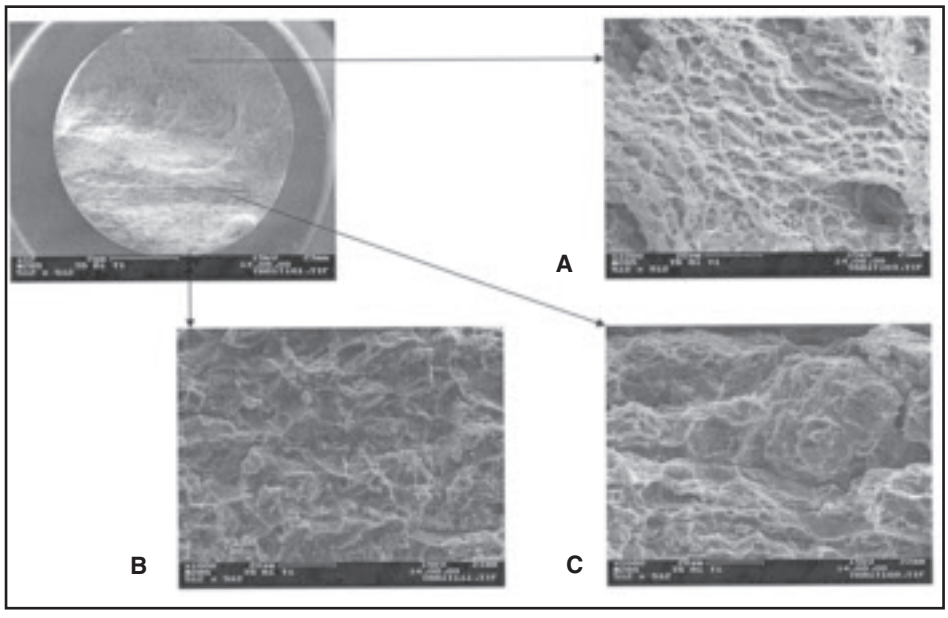

Fig. 12 — Fractograph of broken tensile specimen from weld made at F=167 Hz. A — Fracture through fusion zone first fill pass; B — fracture through weld interface; C — fracture through weld interface.

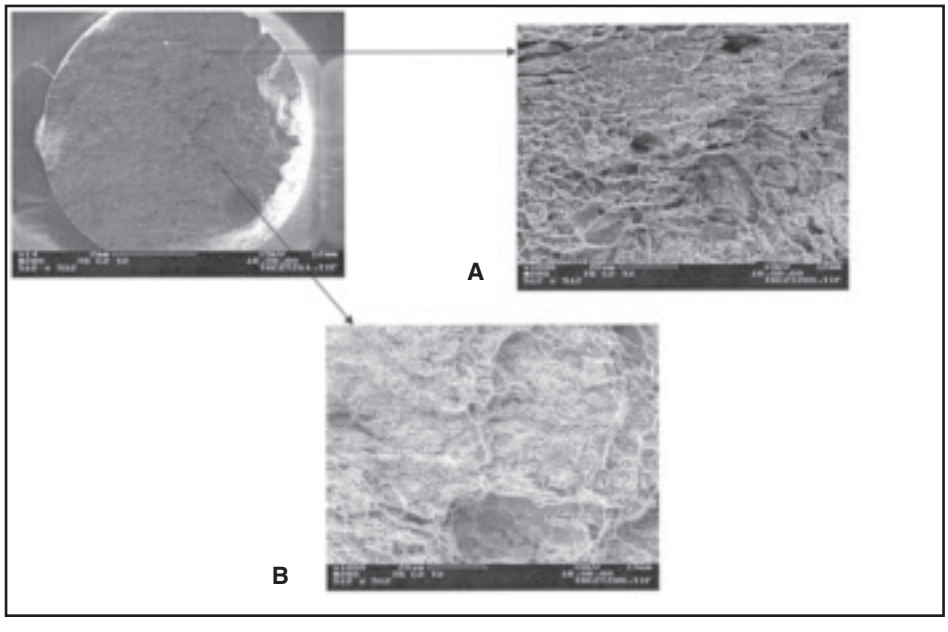

Fig. 13 — Fractograph of broken tensile specimen taken from weld made at F=208 Hz. A —Fracture in fusion zone of fill pass; B — fracture on weld interface/fusion boundary in root pass.

Fatigue and Fracture Toughness Tests

At the time of initiating fatigue precrack for the fracture toughness tests, fatigue crack growth data was stored and the same used to plot the fatigue crack growth curves. Type of specimen used were a standard bend specimen SE(B) as per ASTM A399-90 used for K_{Ic} testing. The crack was oriented in the rolling direction growing in the thickness direction. The tests were conducted on a few base metals (2 or 3 specimens drawn from three different plates) and welded samples. In terms of specimen designation, for example in AlLiT621, AlLi indicates base metal followed by base metal condition T6 in plate number 2 first specimen 1. In the case of welded specimens, T6A1F1 indicates welds made in T6 condition with pulse frequency condition A in welded plate 1 and fracture toughness specimen 1.

An R value of 0.5 was used. Typical log-log plots for da/dN (fatigue crack growth rate) vs. ΔK (cyclic stress intensity factor) for the base metal and the welded metal are shown in Fig. 15. Where a is the crack length, N is number of loading cycles. Generally, da/dN vs. ΔK curves for metallic materials show three distinct regions as shown in Fig. 15A. Region I corresponds to fatigue crack growth threshold ΔK_{th}, which corresponds to the ΔK range below which cracks do not propagate. Region II is for intermediate ΔK where the log-log plot is a straight line, which can be represented by a power law relationship in Equation 7

$$da / dN = C (\Delta K)^m \qquad (7)$$

where C and m are constant for a given material and stress ratio. At high ΔK values, unstable behavior occurs. From the stored fatigue crack growth data, m and C (Paris constants) were obtained by least squares fit of the da/dN vs. ΔK data using the Paris equation. Data in the linear regime (on the log-log plot) are used for fitting such that maximum correlation is obtained. The values are given in Table 8. The observed trend was that m and C are independent of weld parameters used as well as whether it was the base metal or weldment, except for two specimens. Normally m is found between 2 and 4. It is known that m varies between 2 and 4 for many metallic materials. It is also generally known that fatigue crack growth in the Paris region is not influenced by microstructure. The lack of influence is generally attributed to the cyclic plastic zone size being larger than the characteristic microstructural unit size (continuum behavior).

Fracture toughness test (conducted as per ASTM E399-90) results are given in Table 9. Almost independent on the welding parameters, the fracture toughness (K_Q) of the fusion zone is found to be about 13 MPa$\sqrt{m}$ as compared to about 25 MPa$\sqrt{m}$ for the base metal. Upon checking the specimen size adequacy for plane strain fracture toughness, it was found that specimens were not meeting the requirements as per the relevant standards. Hence, the values reported here are regarded as size dependent.

Hardness Survey in T6 Specimens across the Fusion Zone and HAZ

Figure 16 shows the microhardness

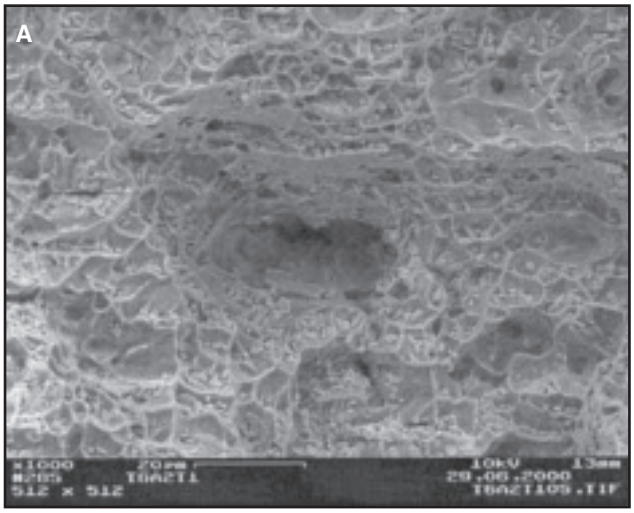

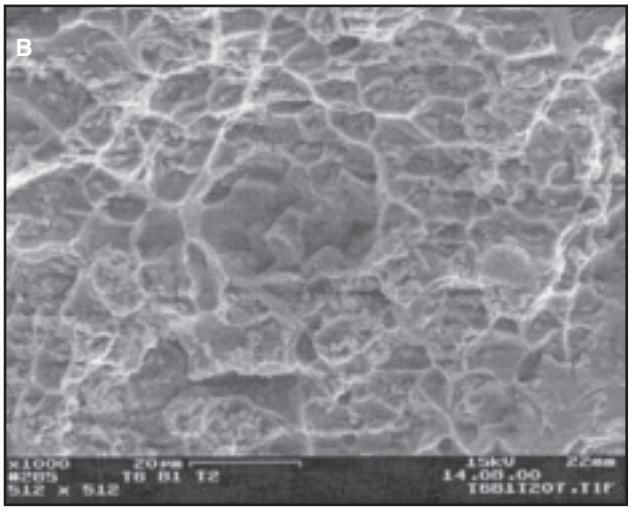

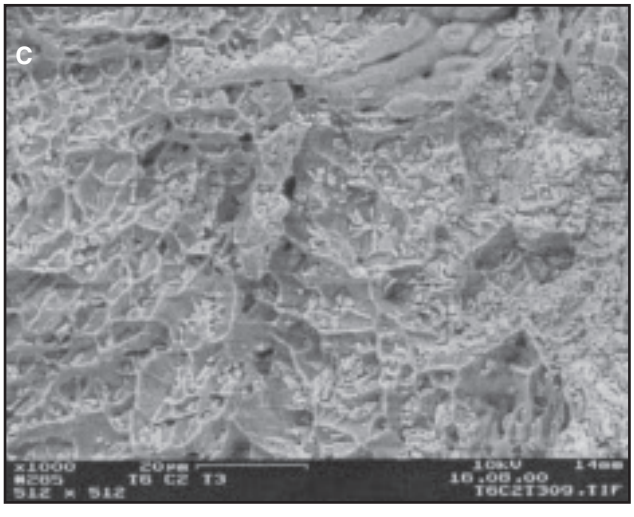

Fig. 14 — Fractographs of fracture through fusion zones of specimens made at different pulse frequencies. A — 125 Hz; B — 167 Hz; C — 208 Hz.

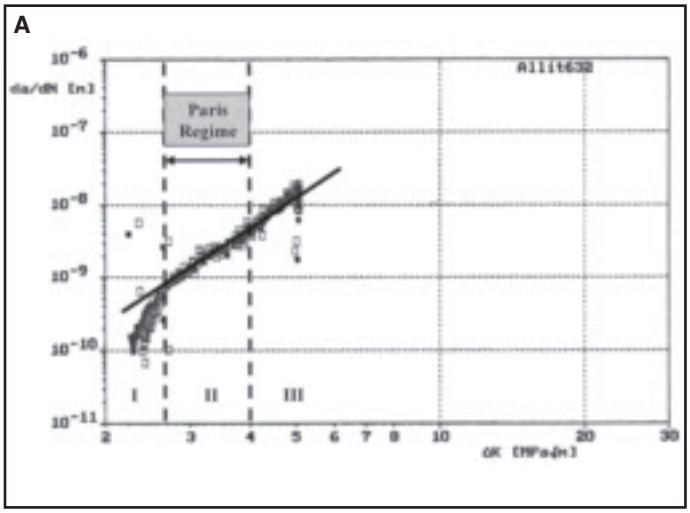

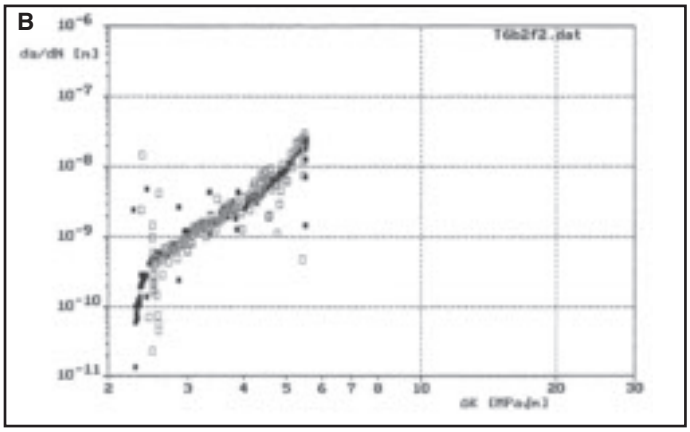

Fig. 15 — Typical fatigue crack growth rate curves. A — Base metal; B — welded specimen.

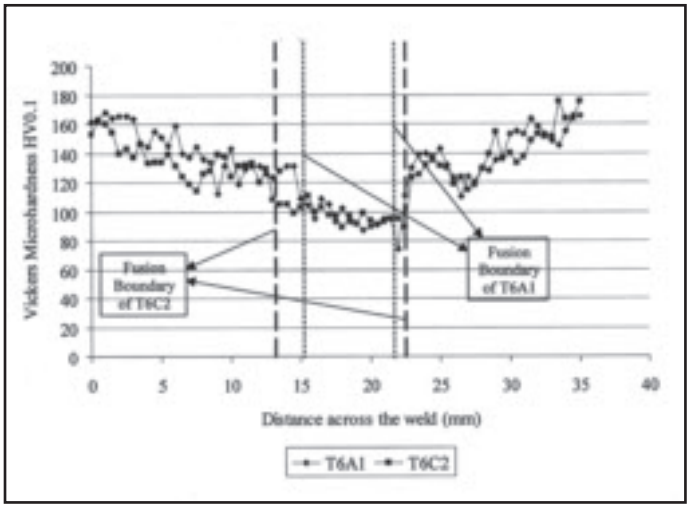

Fig. 16 — Midsection Vickers microhardness profile across the pulsed GMA welds made at pulse frequencies of 167 Hz (T6A1) and 208 Hz (T6C1).

profile across the fusion zone and HAZ of specimens welded in T6 condition at two frequencies 125 and 208 Hz, respectively. The trend seems to be similar to the one reported by other workers (Refs. 28, 29). There is double inflection in the hardness profile from fusion zone through the HAZ. Hardness is low in the fusion zone and steadily increases up to some distance in the HAZ until a peak and then again decreases after which it again increases steadily. It is suggested in their work that it is due to concurrent effects of dissolution and coarsening of precipitates like T_1, θ′, or S′, natural aging due to precipitation of δ′ after welding and diffusion of lithium from HAZ into the weld pool. The first point of inflection (a maximum) corresponds to the point of maximum precipitation of δ′, while the second point of inflection (a minimum) corresponds to the point where the contribution of δ′ and the overaged plate-like precipitate are equal.

Conclusions

1) Welded joints of Al-Cu-Li alloy thick plates made with the GMAW-P process compare well with joints of similar Al-Cu-Li alloys like 2094, 2095, and 2195 in terms of mechanical properties. The GMAW-P process could be considered for welding these types of alloys as thick plates. Since GMAW-P is a less expensive process, many applications could be attempted.

2) Increase in pulse frequency with same mean current and welding speed reduced the yield strength of the joint due to coarsening of weld microstructure. Percentage elongation seems to be increasing slightly, but this may be due to the increase in difference between yield stress and stress at fracture. The tensile properties in specimens made from base metal in T6 or W condition are the same, as the fusion zone mainly governs the properties.

3) Fracture in tensile specimens occurred mostly through the first fill pass and weld interface of the root pass. The fractographs on the weld interface indicated that the fracture could be through the fine equiaxed grain zone or the partially melted zone. So, the fine equiaxed grain zone has an effect on the GMAW-P weldability of Al-Cu-Li alloys. Specimens with large pores had the fracture path following the pores rather than the weld interface. They showed significantly lower fracture stress but yield stress similar to other specimens without large pores.

4) Hardness surveys revealed weaker regions in the fusion zone especially at the boundary between successive weld passes, due to grain coarsening. These microstructural features affect tensile properties. Hardness survey across the fusion zone and heat-affected zone showed the double inflection (a maxima followed by a minima and increase to base metal hardness level) behavior as reported in the literature.

5) Fatigue crack growth behavior in the Paris regime is almost the same in all the specimens, including the base metal. The fracture toughness measured using undersized specimens is found to be almost independent on the welding parameters and amounts to about 13 MPa$\sqrt{m}$ for the fusion zone as compared to about 25 MPa$\sqrt{m}$ for the base metal.

Acknowledgments

The authors acknowledge with thanks the DMRL, Hyderabad, for the alloy, the DAAD for fellowship for work at TU-Dresden, Ing. Zschetzsche (Institute of Production Technology, TU Dresden) for help in welding, and Mrs. Ing. Trommer (Institute of Materials Science, TU Dresden) for help in SEM work.

References

1. Quist, W. H., and Narayanan, G. H. 1989. Aluminum-lithium alloys. *Material Science & Technology*, Vol. 31, p. 219.

2. Irving, B. 1997. Why aren't airplanes welded. *Welding Journal* 76(1): 31–40.

3. Rioja, R. J. 1998. Fabrication methods to manufacture isotropic Al-Li alloys and products for space and aerospace applications. *Materials Science & Engineering* A 257, pp. 100–107.

4. Cross, C. E., and Tack, W. T. 1995. *ASM Metals Handbook*, 10th Ed, Vol. 6, pp. 549–553.

5. Kostrivas, A., and Lippold, J. C. 1999. Weldability of Li-bearing aluminum alloys. *International Materials Reviews*, 446, pp. 217–237.

6. Lippold, J. C. 1989. Weldability of commercial aluminum-lithium alloys, *Proc. of 5th Int. Al-Li Conf.,* Williamsberg, Va. pp. 1365–1375.

7. Pickens, J. R. 1990. Recent developments in the weldability of lithium-containing aluminum alloys. *Journal of Materials Science* 25, pp. 3035–3047.

8. Ellis, M. B. D. 1996. Fusion welding of aluminum-lithium alloys. *Welding & Metal Fabrication* (2): 55–60.

9. Shah, S. R., Wittig, J. E., and Hahn, G. T. 1992. Microstructural analysis of a high strength Al-Cu-Li (Weldalite™ 049) alloy weld. *Proceedings of the 3rd International Conference on Trends in Welding Research*, Gatlinburg, Tenn.

10. Gutierrez, A., and Lippold, J. C. 1998. A proposed mechanism for equiaxed grain formation along the fusion boundary in aluminum-copper-lithium alloys. *Welding Journal* 77(3): 123-s to 132-s.

11. Aidun, K., and Dean, J. P. 1999. Effect of enhanced convection on the microstructure of Al-Cu-Li welds. *Welding Journal* 78(10): 349-s to 354-s.

12. Cornu, J. 1998. Consumable electrode processes. *Advanced Welding Systems*, Vol-II, IFS Publications U.K.

13. Jilong, M., and Apps, R. L. 1982. MIG transfer discovery of importance to industry. *Welding and Metal Fabrication* (9): 307–316.

14. Apps, R. L. 1984. Controlled transfer gas metal arc welding *Proceedings of the International Conference on the Joining of Metals*, (JOM-2), Denmark.

15. Subramaniam, S., White, D. R., Jones, J. E., and Lyons, D. W. 1998. Droplet transfer in pulsed gas metal arc welding of aluminum. *Welding Journal* 77(11): 458-s to 464-s.

16. Rajasekaran, S., Kulkarni, S. D., Mallya, U. D., and Chaturvedi, R. C. 1998. Droplet detachment and plate fusion characteristics in pulsed current gas metal arc welding process. *Welding Journal* 77(6): 254-s to 269-s.

17. Kou, S. 1987. *Welding Metallurgy.* New York, N.Y.: J. Wiley.

18. Kim, I. S., and Basu, A. 1998. A mathematical model of heat transfer and fluid flow in gas metal arc welding process. *J. of Advanced Materials Processing Technology* 77: 17–24.

19. Trindade, E. M., and Allum. 1981. Characteristics in steady and pulsed current GMAW. *Welding and Metal Fabrication* (9): 265–271.

20. Padmanabham, G., Pandey, S., and Schaper, M. 2005. Pulsed-GMAW of an Al-Cu-Li alloy. *Science & Technology of Welding and Joining* 10(1): 67.

21. Padmanabham, G., Pandey, S., and Schaper, M. 2004. Effect of pulse frequency of P-GMAW on weld bead geometry and structure of Al-Cu-Li base plate, *Australasian Welding Journal* 49(3): 33–43.

22. *Metals Handbook,* Vol. 6. 1983. Welding, brazing and soldering – Arc welding of aluminum alloys, ASM International, Materials Park, Ohio.

23. Pandey, S. 1986. PhD thesis, Indian Institute of Technology, Delhi, India.

24. *Proc. of 9th Congress on Materials Testing,* Vol. 1. 1986. F. Schlät, M. Schaper, E. Czoboly, ed., Technoinform, Budapest, pp. 109–113.

25. Chan, K. S. 1993. *Metall. Trans.* A.24A, pp. 2473–2486.

26. Ellis, M. B. D. 1996. Fusion welding of aluminum-lithium alloys. *Welding & Metal Fabrication* (2): 55–60.

27. Strength and fatigue behaviour of fusion joints. 2000. *Proceedings of the German Society for Materials Research* (DVM), Berlin, Germany.

28. Rading, G. O., and Berry, J. T. 1998. A model for heat-affected zone hardness profiles in Al-Li-X alloys. *Welding Journal* 77(9): 383-s to 388-s.

29. Rading, G. O., Shamsuzzoha, M., and Berry, J. T. 1998. A model for HAZ hardness profiles in Al-Li-X alloys: Application to the Al-Li-Cu alloy 2095. *Welding Journal* 77(10): 411-s to 416-s.

30. Reddy, G. M., Gokhale, A. A., Prasad, K. S., and Prasada, R. K. 1998. Chill zone formation in Al-Li alloy welds. *Science & Technology of Welding and Joining* 3(4): 208.